

Computational Tools

Local Perturbation Analysis: A Computational Tool for Biophysical Reaction-Diffusion Models

William R. Holmes,^{1,2,*} May Anne Mata,^{3,4} and Leah Edelstein-Keshet⁵

¹Department of Mathematics, University of Melbourne, Parkville, Australia; ²Center for Mathematical and Computational Biology, Center for Complex Biological Systems, Department of Mathematics, University of California Irvine, Irvine, California; ³I. K. Barber School of Arts and Sciences, University of British Columbia Okanagan, Kelowna, British Columbia, Canada; ⁴Department of Math, Physics, and Computer Science, University of the Philippines Mindanao, Davao City, Philippines; and ⁵Department of Mathematics, University of British Columbia, Vancouver, British Columbia, Canada

ABSTRACT Diffusion and interaction of molecular regulators in cells is often modeled using reaction-diffusion partial differential equations. Analysis of such models and exploration of their parameter space is challenging, particularly for systems of high dimensionality. Here, we present a relatively simple and straightforward analysis, the local perturbation analysis, that reveals how parameter variations affect model behavior. This computational tool, which greatly aids exploration of the behavior of a model, exploits a structural feature common to many cellular regulatory systems: regulators are typically either bound to a membrane or freely diffusing in the interior of the cell. Using well-documented, readily available bifurcation software, the local perturbation analysis tracks the approximate early evolution of an arbitrarily large perturbation of a homogeneous steady state. In doing so, it provides a bifurcation diagram that concisely describes various regimes of the model's behavior, reducing the need for exhaustive simulations to explore parameter space. We explain the method and provide detailed step-by-step guides to its use and application.

INTRODUCTION

Numerous cellular processes are regulated by heterogeneously distributed intracellular proteins that interact in a myriad of functional complexes while also undergoing Brownian motion in the bulk or along the cell surface (1). Because of this, continuum models are often used to describe the spatiotemporal distribution of these subcellular components. These mathematical models often take the form of reaction-diffusion (RD) partial differential equations (PDEs) (2). Indeed, numerous publications in the pages of this journal have included such modeling efforts (3–9). Unfortunately, the analysis required to understand such mathematical models remains challenging even for applied mathematicians. This article describes a recent computational tool for analyzing such systems using readily available bifurcation software. The article is accompanied by user's guides with detailed examples aimed at making the method accessible to a wide range of users.

Complex biochemical networks, typically involving many interacting components, direct spatial organization in cells. A common feature in such systems is the continual binding and unbinding to/from the cell membrane of regulators that have distinct diffusive properties in the bound and unbound states. Systems of this form include small GTPases involved in cell polarization and motility (10), Min proteins

that direct bacterial division (11), Par proteins that partition or polarize in cells (12), and Rop proteins involved in plant cell polarity (13). This ubiquitous class of regulatory systems motivated the development of the method described here.

Reacting and diffusing molecular networks are modeled by medium to large systems of PDEs (6,12,14–21). It is challenging to analyze the repertoire of behaviors and parameter dependence, since even a relatively simple example (Fig. 1) contains ~10 unmeasured parameters and larger circuits have many times more. Understanding the behavior of such systems requires systematic parameter exploration, a daunting computational task.

Applied mathematicians have developed various approximation methods to characterize solutions to PDEs, but such methods are challenging even for small systems of one to two equations; they require substantial expertise to use, and are hardly as universal as bifurcation tools for ordinary differential equations (ODEs). Alternatively, simulations can be effective for exploring small regions of parameter space. Unfortunately, brute force simulation is generally impractical for all but the simplest systems. Here, we describe a computational tool, Local Perturbation Analysis (LPA), originally devised by A. F. M. Marée and Veronica Grieneisen (14,22) and developed further in our group (20,23–26) as an aid in such PDE analysis. The benefits of this tool are twofold. First, it provides a concise overview of the regimes of patterning behavior in a single diagram. Second, it is much more computationally tractable than

Submitted September 4, 2014, and accepted for publication November 6, 2014.

*Correspondence: holmesw@unimelb.edu.au

Editor: Stanislav Shvartsman.

© 2015 by the Biophysical Society
0006-3495/15/01/0230/7 \$2.00

<http://dx.doi.org/10.1016/j.bpj.2014.11.3457>



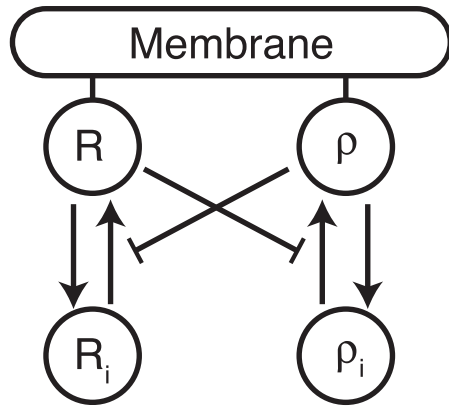


FIGURE 1 A mutually inhibitory circuit of the small GTPases Rac and Rho. Each one cycles between a membrane-bound active (R, ρ) and cytosolic inactive (R_i, ρ_i) form. Each active GTPase inhibits the activation of its antagonist.

existing methods. Although this approach has been implemented previously and the method and its applicability have been described, to our knowledge, we provide the first practical, user-friendly guides (included as [Supporting Material](#)) based on readily available software packages (Matlab-based Matcont (27) (Mathworks, Natick, MA) and the freeware XPPAUT).

MATERIALS AND METHODS

It is well-known that nonlinear RD systems of two or more components can give rise to pattern formation and complex spatiotemporal dynamics (28). At its simplest, a pair of pattern-forming RD equations has the form

$$\frac{\partial u}{\partial t}(x, t) = f(u, v; p) + D_u u_{xx}, \quad (1a)$$

$$\frac{\partial v}{\partial t}(x, t) = g(u, v; p) + D_v v_{xx}, \quad (1b)$$

where f and g are typically nonlinear functions of the chemical concentrations u and v . Here, p is some parameter of interest, and $D_u \ll D_v$ is assumed. Note that although a difference of diffusivities is commonly required for pattern formation, the large size of the discrepancy assumed here is motivated by systems involving regulators that diffuse in the bulk (fast) or along the cell membrane (slow), where rates of diffusivity can differ by a factor of 100–1000. This is a central requirement for application of the LPA method. Thus, from here on, we assume that all molecular regulators can be grouped into one of two classes: slow-diffusing (u) or fast-diffusing (v). We will further assume that the system being studied is a closed system, employing no-flux boundary conditions, and that the domain is small enough that fast-diffusing regulators can be considered to be homogeneously distributed.

The LPA principally addresses the following question: for a given parameter (p) or parameter range $p_1 \leq p \leq p_2$, will a stimulus applied to a cell elicit a patterning response? This is a canonical stability question. Standard ODE bifurcation techniques assess the stability of a state to global, well-mixed perturbations. Turing analysis probes stability with respect to small-amplitude spatial perturbations. However, these methods are not well suited to determine how a system will respond to larger-amplitude spatial stimuli. To address this issue, the LPA tracks the evolution of a large-amplitude,

localized pulse (perturbation) that has very narrow width and, hence, negligible mass. This is, of course, not a physiological stimulus, but it provides a number of mathematical conveniences that can be exploited to simplify matters. Since u is slowly diffusing, the height of this pulse can be represented by a single local variable, $u^l(t)$, that does not spatially spread. Due to the fast rate of diffusion, v can be represented by a uniform, global quantity, $v^g(t)$, on the entire domain. Since u does not spread and v is uniform on the domain, u can then be represented on the remainder of the domain (away from the perturbation) by a global quantity, $u^g(t)$. See our previous work (24) for further details. In the limit of a large diffusion disparity ($D_u \ll D_v$), the evolution of these quantities is described by

$$\frac{du^g}{dt}(x, t) = f(u^g, v^g; p), \quad (2a)$$

$$\frac{dv^g}{dt}(x, t) = g(u^g, v^g; p), \quad (2b)$$

$$\frac{du^l}{dt}(x, t) = f(u^l, v^g; p). \quad (2c)$$

The advantage of this approximation is that the resulting set of ODEs can be handled by available ODE bifurcation software. This substantially reduces the mathematical and computational complexity of probing the nonlinear behavior of patterning systems. As we show, the results of such analysis lead to insight about how one or more parameters of interest affect the fate of the pulse.

RESULTS

We provide several examples of this computational tool in order of increasing complexity. Tutorials and codes are provided as a step-by-step guide for the user.

Example 1: the Schnakenberg system

This simple pattern-forming prototype (see Murray (29)) consists of RD equation system 1 (Eqs. 1a and 1b). with kinetics

$$f(u, v) = a - u + u^2v, \quad g(u, v) = b - u^2v. \quad (3)$$

The corresponding LPA equations for u^l, u^g, v^g are formulated by plugging these expressions for f, g into equation system 2 (Eqs. 2a–2c). In this case, the LPA equations have analytically solvable steady-state (SS) solutions:

$$u^l = a + b, u^g = a + b, v^g = \frac{b}{(a + b)^2}, \quad (4a)$$

$$u^l = a + \frac{a^2}{b}, u^g = a + b, v^g = \frac{b}{(a + b)^2}. \quad (4b)$$

The first of these (Eq. 4a) represents homogeneous solutions of the well-mixed system of equations (i.e., $u^l = u^g$), whereas the second (Eq. 4b) provides information about patterning properties.

Fig. 2 illustrates one- and two-parameter bifurcation diagrams of the reduced LPA system, summarizing parameter-dependent behavior. In Fig. 2 a, the black lines indicate the global steady state (stable, *solid lines*; unstable, *dashed lines*). The gray curve is the local branch (where $u^l \neq u^g$), and superimposed arrows describe the growth (upward) or decay (downward) of the local pulse. For $a = 2$, with b the bifurcation parameter, we find a change in behavior (transcritical bifurcation) at $b = 2$. In the spontaneous regime, the globally uniform steady state is unstable to arbitrarily small perturbations (i.e., linearly unstable). In the stimulus-induced regime, that state is stable against small perturbations, but perturbations above some threshold (*dashed gray line*) will elicit a response. Fig. 2 b is a two-parameter bifurcation diagram showing the boundary ($a = b$) between the two regimes, which can be determined analytically in this case or, more generally, by numerically continuing the branch point between different regimes (24). Numerical simulations (not shown) and previous analysis (29) confirm these results. The example demonstrates that LPA can provide a concise overview of the linear and nonlinear properties of a system.

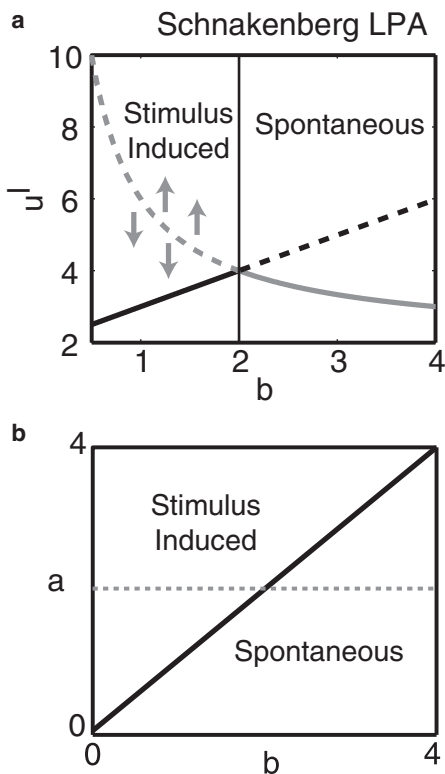


FIGURE 2 (a) LPA bifurcation diagram for the Schnakenberg system. The black branch is the homogeneous steady-state solution, $u^l = u^g$, and the gray branch represents local solutions of the LPA-ODEs $u^l \neq u^g$. In the spontaneous regime, any departure from the homogeneous steady state induces a response. In the stimulus-induced regime, large amplitude stimuli are required to incite a response. (b) A two-parameter LPA bifurcation plot, showing the two regimes as a function of input parameters (a, b). The gray line shows a slice through this plane at $a = 2$, which corresponds to a .

Example 2: the Gierer-Meinhardt model

A well-known pattern-forming system consists of RD equation system 1 (Eqs. 1a and 1b) with kinetics

$$f(u, v) = a - bu + \frac{u^2}{v(1 + ku^2)}, \quad g(u, v) = u^2 - v. \quad (5)$$

This system is not analytically tractable but is easily amenable to LPA. The reduced LPA equations are equation system 2 with the kinetics of Eq. 5. LPA analysis of this system (Fig. 3 a) indicates three regimes, including stimulus-induced patterning (III), a Turing instability (II), and Turing-Hopf instability (implying cycles) (I). We verified each regime using full PDE simulations. For example, Fig. 3 b shows a time-periodic oscillating polar distribution in kymograph view, as predicted in region I. This example shows that LPA can detect some exotic changes of behavior, such as Turing-Hopf bifurcations, predicting the onset of cycles.

Example 3: the Rac-Rho system

A mutually inhibitory circuit of two components often appears in cell signaling models. Here, we consider

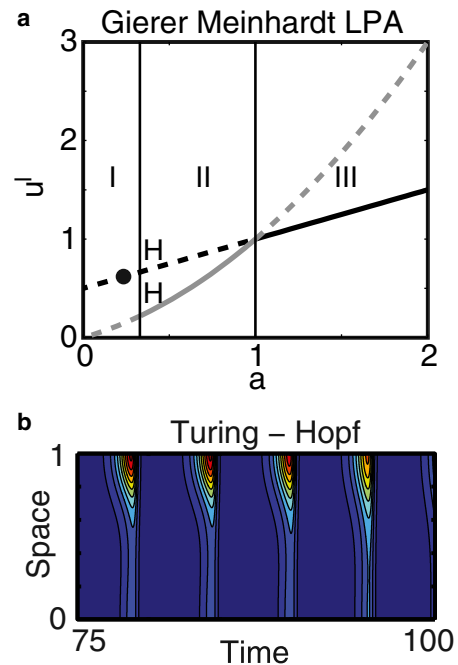


FIGURE 3 (a) LPA diagram for the Gierer-Meinhardt system. In Region III, the HSS is linearly stable, but under certain diffusion conditions, a large-amplitude pulse will give rise to patterning. A stationary Turing instability is present in Region II. Region I is a Turing-Hopf regime where both Turing and Hopf instabilities co-occur. Parameter values used are $b = 2$ and $K = 0$. (b) Example of an oscillating pattern from Region I (at the value of parameter a marked by the dot in a), demonstrating the predicted interaction between Turing and Hopf instabilities. Domain size is 1 with $D_v = 1, D_u = 0.01$. To see this figure in color, go online.

interactions between Rac and Rho (Fig. 1); other systems such as PAR proteins interact in similar ways (12). Each of these proteins has both a membrane-associated active form (R, ρ) and a cytosolic inactive form (R_i, ρ_i). This leads to the large disparity in rates of diffusion exploited by LPA. Since the total amount of a component is fixed (e.g., $\int_0^L [R(x, t) + R_i(x, t)] dx = R_{\text{tot}} = \text{constant}$), some care is needed in the LPA reduction, as discussed in the Appendix.

A typical bifurcation diagram (Fig. 4) illustrates three regimes of behavior. In Region I, the homogeneous steady state (HSS) is linearly stable, but large stimuli provoke a response. As basal Rac activation strength (k_R , the bifurcation parameter) increases, the response threshold decreases to zero, so that in Region II, arbitrarily small perturbations will incite a response (a linearly unstable regime). For yet larger values of $k_R > 0.4$ (region III), the system is uniformly activated (indicated by the increased Rac level of the HSS), and no perturbation can provoke a response. At other parameter values, there can be more than one type of stimulus-response regime, triggered by pulses of either activation or deactivation (see XPPAUT tutorial, Example 3). Full RD simulations confirm such predictions.

Example 4: analysis of a yeast-bud polarization model

To illustrate the adaptability of LPA, we next consider an example with more biological detail (and hence more equations and parameters), namely, the yeast polarization/budding signaling model (19), as described in (30–32) (Fig. 5 a). This model tracks Cdc42, its activator Bem1, and a guanine disassociation inhibitor (GDI) in the set of eight RD equations (Eqs. 9a–9h in the Appendix; for details, see Goryachev and Pokhilko (19) and Layton et al. (31)). The activate-inactivate, cytosolic and membrane-bound

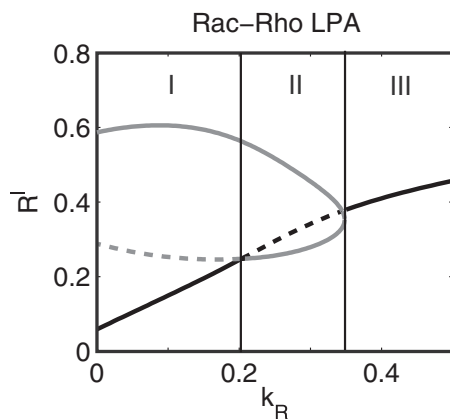


FIGURE 4 LPA diagram for the mutually inhibitory Rac-Rho circuit shown in Fig. 1 and given by RD equation system 6 (Eqs. 6a and 6b). The LPA system is equation system 8 (Eqs. 8a and 8b) with parameters: $a_1 = a_2 = 0.25, n = 3, k_p = 0.2, I_R = 0.7, \delta_R = \delta_p = I_p = R_{\text{tot}} = \rho_{\text{tot}} = 1$. Marked regions correspond to stimulus-induced (I), linearly unstable (II), and completely stable (III, i.e., no patterning possible) parameter regimes.

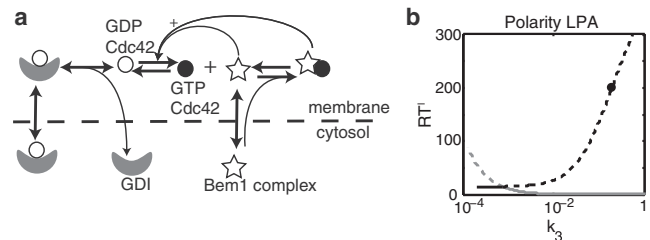


FIGURE 5 (a) Schematic diagram for the yeast budding polarity model, adapted from Savage et al. (32). Cytosolic components are fast, whereas membrane-bound components are slow. (b) LPA diagram for the yeast polarity model from Savage et al. (32). RT^1 indicates the local variable describing active Cdc42 concentration, which indicates bud location, and all parameters other than k_3 , as in Layton et al. (31). Black and gray curves represent well mixed and perturbed states, respectively. The heavy dot corresponds to k_3 , as in Layton et al. (31).

states, and bound complexes are grouped into fast/slow components, as before, in the LPA reduction to ODEs. In Goryachev and Pokhilko (19) and Savage et al. (32), the cell is spherical, with a homogeneous interior (cytosol). The geometry must be considered in formulating three conservation laws required by the LPA reduction (to avoid issues with zero eigenvalues, see the Appendix).

Despite increased complexity, applying LPA is straightforward as before. This leads to $2 \times 5 + 1 \times 3 = 13$ ODEs for five membrane-bound (slow) variables (each represented by local and global variables) and three cytosolic (fast) variables (depicted by one global variable each). The three conserved quantities in the system lead to three algebraic constraints, eliminating three ODEs for global variables.

Based on Goryachev and Pokhilko (19), a critical autocatalytic loop involving the complex Cdc42-Bem1-Cdc24 activating Cdc42 is needed for instability. We thus consider the parameter k_3 , which governs the strength of that autocatalysis, as the bifurcation parameter. LPA results indicate that the system is linearly stable for small k_3 but that a sufficiently large perturbation would give rise to a response. As this parameter increases, the threshold required for a response decreases until the bifurcation is reached and the system becomes unstable. These results further indicate that this instability persists over at least five orders of magnitude for this parameter (originally $k_3 = 0.35$ in Layton et al. (31) (Fig. 5 b, black dot)), suggesting robustness of polarity. Fig. 5 b shows that the Turing stability is only lost at $k_3 \approx 7 \times 10^{-4}$ and continuation to higher k_3 (not shown) shows the instability persists to at least $k_3 = 10^2$.

DISCUSSION

Over the past two decades, as computational capabilities have improved, a number of biological markup languages (e.g., SBML (33) and CellML (34)) and model simulation packages (e.g., Virtual Cell (35) CHASTE (36), and CompuCell3D (37)) have been developed. Although these have somewhat democratized the development and simulation

of complex biological models, the problem of deciphering the predictions of such models remains a challenge. In particular, understanding and summarizing the behavior of a given system in a compact and informative way remains difficult.

Linear (Turing) stability analysis can illuminate the presence of spontaneous pattern formation in RD systems of a few interacting components but provides no information about stimulus-driven and threshold-dependent cellular responses. Nonlinear analysis methods provide much more detailed information (38–40) but are very difficult to implement and can rarely be applied to real systems of even moderate complexity. Massive random exploration of parameter space (e.g., Chau et al. (41)), an alternate approach, is computationally costly. Here, we surveyed a relatively new and simple computational tool, not yet widely known, that aids analysis of complex regulatory networks governing spatial organization.

As we have shown, LPA, designed to analyze systems of reacting diffusing regulators, exploits the large disparity in rates of diffusion to provide information about early time evolution of stimuli (arbitrarily large localized perturbations). Although the factor of 100–1000 difference in diffusivities, common in cellular systems, is sufficiently large for this method to be predictive, we do note that this is an approximation method. The location of predicted bifurcations is not precise, and the size of patterning regimes generally shrinks as you move away from this limiting regime. Thus, simulations are still needed to verify results and characterize the specific form of solutions to the PDEs. The LPA tests do, however, vastly cut down the time and effort needed to initially explore a model. This method predicts the number of distinct phenotypic regimes as any parameter is varied, as well as the approximate location of bifurcations between them. In our own investigations of signaling pathways, this tool has guided development of the models, their parametrization, and interpretation of mutations, knock-outs, or overexpression experiments. We present this summary because we believe that this computational tool will have wide applicability in biophysical research.

APPENDIX

Example 3 model equations

The PDEs for the Rac-Rho mutual inhibition system are as follows:

$$\begin{aligned} \frac{\partial R}{\partial t}(x, t) &= f(R, \rho, R_i) + DR_{xx}, \\ \frac{\partial R_i}{\partial t}(x, t) &= -f(R, \rho, R_i) + D_i(R_i)_{xx} \end{aligned} \quad (6a)$$

$$\begin{aligned} \frac{\partial \rho}{\partial t}(x, t) &= g(R, \rho, \rho_i) + D\rho_{xx}, \\ \frac{\partial \rho_i}{\partial t}(x, t) &= -g(R, \rho, \rho_i) + D_i(\rho_i)_{xx}, \end{aligned} \quad (6b)$$

where R, ρ and R_i, ρ_i are active membrane-bound and inactive cytosolic forms, respectively, so that $D_i \gg D$. Typical kinetics are

$$\begin{aligned} f(R, \rho, R_i) &= \left(k_r + \frac{I_r}{1 + (\rho/a_1)^n} \right) \frac{R_i}{R_{\text{tot}}} - d_r R, \\ g(R, \rho, \rho_i) &= \left(k_\rho + \frac{I_\rho}{1 + (R/a_2)^n} \right) \frac{\rho_i}{\rho_{\text{tot}}} - d_\rho \rho. \end{aligned}$$

The system satisfies conservation ($\int_0^L [R(x, t) + R_i(x, t)] dx = LR_{\text{tot}} = \text{constant}$), so that any uniform steady state can be characterized by $R + R_i = R_{\text{tot}}$. In the LPA system, active slow components are represented by both their local and global levels (R^l, R^g and similarly for ρ), whereas inactive fast forms have a single global representation (R_i^g , and similarly for ρ). This leads to the LPA system

$$\begin{aligned} \frac{\partial R^l}{\partial t} &= f(R^l, \rho^l, R_i^g), & \frac{\partial R^g}{\partial t} &= f(R^g, \rho^g, R_i^g), \\ \frac{\partial R_i^g}{\partial t} &= -f(R^g, \rho^g, R_i^g), \end{aligned} \quad (7a)$$

$$\begin{aligned} \frac{\partial \rho^l}{\partial t} &= g(R^l, \rho^l, \rho_i^g), & \frac{\partial \rho^g}{\partial t} &= g(R^g, \rho^g, \rho_i^g), \\ \frac{\partial \rho_i^g}{\partial t} &= -g(R^g, \rho^g, \rho_i^g). \end{aligned} \quad (7b)$$

However, an additional step is required in this example. Conservation of each form leads to one eigenvalue, $\lambda = 0$, for equation system 7 (Eqs. 7a and 7b), which is problematic for bifurcation software. Hence, the system is first reduced by eliminating the inactive variables using the (algebraic) conservation statements (e.g., $R_i^g = R_{\text{tot}} - R^g$). This leads to the smaller system

$$\begin{aligned} \frac{\partial R^l}{\partial t} &= f(R^l, \rho^l, (R_{\text{tot}} - R^g)), \\ \frac{\partial R^g}{\partial t} &= f(R^g, \rho^g, (R_{\text{tot}} - R^g)) \end{aligned} \quad (8a)$$

$$\begin{aligned} \frac{\partial \rho^l}{\partial t} &= g(R^l, \rho^l, (\rho_{\text{tot}} - \rho^g)), \\ \frac{\partial \rho^g}{\partial t} &= g(R^g, \rho^g, (\rho_{\text{tot}} - \rho^g)). \end{aligned} \quad (8b)$$

Example 4 model equations

The model in Fig. 5 a consists of a set of PDEs. The variables (in concentration units) are RT = active Cdc42, M = Cdc42-Bem1-Cdc24 complex, E_m = Bem1-Cdc24 complex on the membrane, E_c = Bem1-Cdc24 complex in the cytosol, RD = inactive membrane bound Cdc42, RDI_m = inactive Cdc42-GDI complex bound to the membrane, RDI_c = inactive Cdc42-GDI complex in the cytosol, and I = GDI. The kinetic terms and parameter values are taken directly from Layton et al. (31).

$$\frac{\partial RT}{\partial t} = f_{RT}(E_m, M, RD, RT, E_c) + D_m \Delta RT, \quad (9a)$$

$$\frac{\partial M}{\partial t} = f_M(E_m, RT, M, E_c) + D_m \Delta M, \quad (9b)$$

$$\frac{\partial E_m}{\partial t} = f_{E_m}(E_c, E_m, RT, M) + D_m \Delta E_m, \quad (9c)$$

$$\frac{\partial E_c}{\partial t} = \eta f_{E_c}(E_m, RT, E_c) + D_c \Delta E_c, \quad (9d)$$

$$\frac{\partial RD}{\partial t} = f_{RD}(RT, E_m, M, RD, RDI_m, I) + D_m \Delta RD, \quad (9e)$$

$$\frac{\partial RDI_m}{\partial t} = f_{RDIm}(I, RD, RDI_m, RDI_c) + D_m \Delta RDI_m, \quad (9f)$$

$$\frac{\partial RDI_c}{\partial t} = \eta f_{RDIC}(RDI_m, RDI_c) + D_c \Delta RDI_c, \quad (9g)$$

$$\frac{\partial I}{\partial t} = \eta f_I(RDI_m, RD, I) + D_c \Delta I. \quad (9h)$$

The LPA equations are 13 ODEs. However, three conserved quantities (19) would lead to three degenerate eigenvalues in the linearization. As before, to avoid crashing the bifurcation software, the following algebraic conservation statements are used to eliminate three variables:

$$RDI_c^g = (1 + \eta)R_0 - \eta(RT^g + RD^g + M^g + RDI_m^g), \quad (10a)$$

$$E_c^g = (1 + \eta)E_0 - \eta(E_m^g + M^g), \quad (10b)$$

$$I^g = (1 + \eta)I_0 - \eta RDI_m^g - RDI_c^g. \quad (10c)$$

The prefactor here accounts for the large discrepancy between membrane and cytosolic volume $\eta = V_m / V_c \sim 0.01$, where $V_{m,c}$ denote those volumes. The quantities R_0, E_0, I_0 represent conserved mean concentrations of Cdc42, Bem1, and GDI, respectively. That is, the total conserved amount of Cdc42 for example (in all its forms and complexes) is $(V_m + V_c)R_0$. The resulting system of 10 LPA ODEs is then

$$\frac{dRT^l}{dt} = f_{RT}(E_m^l, M^l, RD^l, RT^l, E_c^g), \quad (11a)$$

$$\frac{dRT^g}{dt} = f_{RT}(E_m^g, M^g, RD^g, RT^g, E_c^g),$$

$$\begin{aligned} \frac{dM^l}{dt} &= f_M(E_m^l, RT^l, M^l, E_c^g), \\ \frac{dM^g}{dt} &= f_M(E_m^g, RT^g, M^g, E_c^g), \end{aligned} \quad (11b)$$

$$\begin{aligned} \frac{dE_m^l}{dt} &= f_{E_m}(E_c^g, E_m^l, RT^l, M^l), \\ \frac{dE_m^g}{dt} &= f_{E_m}(E_c^g, E_m^g, RT^g, M^g), \end{aligned} \quad (11c)$$

$$\begin{aligned} \frac{dRD^l}{dt} &= f_{RD}(RT^l, E_m^l, M^l, RD^l, RDI_m^l, I^g), \\ \frac{dRD^g}{dt} &= f_{RD}(RT^g, E_m^g, M^g, RD^g, RDI_m^g, I^g), \end{aligned} \quad (11d)$$

$$\begin{aligned} \frac{dRDI_m^l}{dt} &= f_{RDIm}(I^g, RD^l, RDI_m^l, RDI_c^g), \\ \frac{dRDI_m^g}{dt} &= f_{RDIm}(I^g, RD^g, RDI_m^g, RDI_c^g), \end{aligned} \quad (11e)$$

where the ODEs for the three cytosolic variables have been replaced by the corresponding constraints (10).

SUPPORTING MATERIAL

A guide to LPA with XPP and a guide to LPA with MatLab-based MatCont are available at [http://www.biophysj.org/biophysj/supplemental/S0006-3495\(14\)04670-0](http://www.biophysj.org/biophysj/supplemental/S0006-3495(14)04670-0).

ACKNOWLEDGMENTS

We are grateful to Danny Lew and Anita Layton for providing equations, parameter values, and other details for their yeast bud polarization model. We also thank Stan Maree and Veronica Grieneisen for discussions about LPA.

While working together at the University of British Columbia, all authors were supported by an National Sciences and Engineering Research Council Discovery grant to L.E.K. W.R.H. was also supported by National Institutes of Health grant P50GM76516 while at the University of California Irvine.

REFERENCES

- Gerisch, G., T. Bretschneider, ..., K. Anderson. 2004. Mobile actin clusters and traveling waves in cells recovering from actin depolymerization. *Biophys. J.* 87:3493–3503.
- Maini, P., K. Painter, and H. Chau. 1997. Spatial pattern formation in chemical and biological systems. *J. Chem. Soc. Faraday Trans.* 93:3601–3610.
- Levchenko, A., and P. A. Iglesias. 2002. Models of eukaryotic gradient sensing: application to chemotaxis of amoebae and neutrophils. *Biophys. J.* 82:50–63.
- Bretschneider, T., K. Anderson, ..., G. Gerisch. 2009. The three-dimensional dynamics of actin waves, a model of cytoskeletal self-organization. *Biophys. J.* 96:2888–2900.
- Enculescu, M., M. Sabouri-Ghomi, ..., M. Falcke. 2010. Modeling of protrusion phenotypes driven by the actin-membrane interaction. *Biophys. J.* 98:1571–1581.
- Ma, L., C. Janetopoulos, ..., P. A. Iglesias. 2004. Two complementary, local excitation, global inhibition mechanisms acting in parallel can explain the chemoattractant-induced regulation of PI(3,4,5)P3 response in dictyostelium cells. *Biophys. J.* 87:3764–3774.
- Machacek, M., and G. Danuser. 2006. Morphodynamic profiling of protrusion phenotypes. *Biophys. J.* 90:1439–1452.
- Mori, Y., A. Jilkine, and L. Edelstein-Keshet. 2008. Wave-pinning and cell polarity from a bistable reaction-diffusion system. *Biophys. J.* 94:3684–3697.
- Ryan, G. L., H. M. Petrocchia, ..., D. Vavylonis. 2012. Excitable actin dynamics in lamellipodial protrusion and retraction. *Biophys. J.* 102:1493–1502.

10. Jilkine, A., and L. Edelstein-Keshet. 2011. A comparison of mathematical models for polarization of single eukaryotic cells in response to guided cues. *PLoS Comput. Biol.* 7:e1001121.
11. Huang, K. C., Y. Meir, and N. S. Wingreen. 2003. Dynamic structures in *Escherichia coli*: spontaneous formation of MinE rings and MinD polar zones. *Proc. Natl. Acad. Sci. USA.* 100:12724–12728.
12. Goehring, N. W., P. K. Trong, ..., S. W. Grill. 2011. Polarization of PAR proteins by advective triggering of a pattern-forming system. *Science.* 334:1137–1141.
13. Fu, Y., and Z. Yang. 2001. Rop GTPase: a master switch of cell polarity development in plants. *Trends Plant Sci.* 6:545–547.
14. Jilkine, A., A. F. Marée, and L. Edelstein-Keshet. 2007. Mathematical model for spatial segregation of the Rho-family GTPases based on inhibitory crosstalk. *Bull. Math. Biol.* 69:1943–1978.
15. Marée, A. F., A. Jilkine, ..., L. Edelstein-Keshet. 2006. Polarization and movement of keratocytes: a multiscale modelling approach. *Bull. Math. Biol.* 68:1169–1211.
16. Levine, H., D. A. Kessler, and W.-J. Rappel. 2006. Directional sensing in eukaryotic chemotaxis: a balanced inactivation model. *Proc. Natl. Acad. Sci. USA.* 103:9761–9766.
17. Dawes, A. T., and L. Edelstein-Keshet. 2007. Phosphoinositides and Rho proteins spatially regulate actin polymerization to initiate and maintain directed movement in a one-dimensional model of a motile cell. *Biophys. J.* 92:744–768.
18. Otsuji, M., S. Ishihara, ..., S. Kuroda. 2007. A mass conserved reaction-diffusion system captures properties of cell polarity. *PLoS Comput. Biol.* 3:e108.
19. Goryachev, A. B., and A. V. Pokhilko. 2008. Dynamics of Cdc42 network embodies a Turing-type mechanism of yeast cell polarity. *FEBS Lett.* 582:1437–1443.
20. Holmes, W. R., B. Lin, ..., L. Edelstein-Keshet. 2012. Modelling cell polarization driven by synthetic spatially graded Rac activation. *PLoS Comput. Biol.* 8:e1002366.
21. Marée, A. F., V. A. Grieneisen, and L. Edelstein-Keshet. 2012. How cells integrate complex stimuli: the effect of feedback from phosphoinositides and cell shape on cell polarization and motility. *PLoS Comput. Biol.* 8:e1002402.
22. Grieneisen, V. 2009. Dynamics of auxin patterning in plant morphogenesis. PhD thesis, University of Utrecht, Utrecht, The Netherlands.
23. Mata, M. A., M. Dutot, ..., W. R. Holmes. 2013. A model for intracellular actin waves explored by nonlinear local perturbation analysis. *J. Theor. Biol.* 334:149–161.
24. Holmes, W. R. 2014. An efficient, nonlinear stability analysis for detecting pattern formation in reaction diffusion systems. *Bull. Math. Biol.* 76:157–183.
25. Holmes, W. R., A. E. Carlsson, and L. Edelstein-Keshet. 2012. Regimes of wave type patterning driven by refractory actin feedback: transition from static polarization to dynamic wave behaviour. *Phys. Biol.* 9:046005.
26. Lin, B., W. R. Holmes, ..., A. Levchenko. 2012. Synthetic spatially graded Rac activation drives cell polarization and movement. *Proc. Natl. Acad. Sci. USA.* 109:E3668–E3677.
27. Dhooge, A., W. Govaerts, and Y. Kuznetsov. 2003. Matcont: A Matlab package for numerical bifurcation analysis of ODEs. *ACM Trans. Math. Softw.* 29:141–164.
28. Turing, A. 1952. The chemical basis of morphogenesis. *Philos. Trans. Roy. Soc. Lond. B Biol. Sci.* 237:37–72.
29. Murray, J. 2003. *Mathematical Biology: Spatial Models and Biomedical Applications*, volume 2. Springer-Verlag, New York.
30. Kuo, C.-C., N. S. Savage, ..., D. J. Lew. 2014. Inhibitory GEF phosphorylation provides negative feedback in the yeast polarity circuit. *Curr. Biol.* 24:753–759.
31. Layton, A. T., N. S. Savage, ..., D. J. Lew. 2011. Modeling vesicle traffic reveals unexpected consequences for Cdc42p-mediated polarity establishment. *Curr. Biol.* 21:184–194.
32. Savage, N. S., A. T. Layton, and D. J. Lew. 2012. Mechanistic mathematical model of polarity in yeast. *Mol. Biol. Cell.* 23:1998–2013.
33. Keating, S. M., B. J. Bornstein, ..., M. Hucka. 2006. SBMLToolbox: an SBML toolbox for MATLAB users. *Bioinformatics.* 22:1275–1277.
34. Lloyd, C. M., M. D. Halstead, and P. F. Nielsen. 2004. CellML: its future, present and past. *Prog. Biophys. Mol. Biol.* 85:433–450.
35. Loew, L. M., and J. C. Schaff. 2001. The Virtual Cell: a software environment for computational cell biology. *Trends Biotechnol.* 19:401–406.
36. Mirams, G. R., C. J. Arthurs, ..., D. J. Gavaghan. 2013. Chaste: an open source C++ library for computational physiology and biology. *PLoS Comput. Biol.* 9:e1002970.
37. Swat, M. H., G. L. Thomas, ..., J. A. Glazier. 2012. Multi-scale modeling of tissues using CompuCell3D. *Methods Cell Biol.* 110:325–366.
38. Iron, D., and M. Ward. 2000. A metastable spike solution for a nonlocal reaction diffusion model. *SIAM J. Appl. Math.* 60:778–802.
39. Mori, Y., A. Jilkine, and L. Edelstein-Keshet. 2011. Asymptotic and bifurcation analysis of wave-pinning in a reaction-diffusion model for cell polarization. *SIAM J. Appl. Math.* 71:1401–1427.
40. Rubinstein, B., B. D. Slaughter, and R. Li. 2012. Weakly nonlinear analysis of symmetry breaking in cell polarity models. *Phys. Biol.* 9:045006.
41. Chau, A. H., J. M. Walter, ..., W. A. Lim. 2012. Designing synthetic regulatory networks capable of self-organizing cell polarization. *Cell.* 151:320–332.